Bio-Design and Manufacturing (2019) 2:242–255
https://doi.org/10.1007/s42242-019-00054-7

RESEARCH ARTICLE

The effect of porosity on the mechanical properties of 3D-printed triply periodic minimal surface (TPMS) bioscaffold

Zizhen Cai[1] · Zehua Liu[1] · Xiaodong Hu[1] · Hekun Kuang[1] · Jinsong Zhai[1]

Received: 19 September 2019 / Accepted: 21 October 2019 / Published online: 5 November 2019

Abstract

Prevailing tissue degeneration caused by musculoskeletal maladies poses a great demand on bioscaffolds, which are artificial, biocompatible structures implanted into human bodies with appropriate mechanical properties. Recent advances in additive manufacturing, i.e., 3D printing, facilitated the fabrication of bioscaffolds with unprecedented geometrical complexity and size flexibility and allowed for the fabrication of topologies that would not have been achieved otherwise. In our work, we explored the effect of porosity on the mechanical properties of a periodic cellular structure. The structure was derived from the mathematically created triply periodic minimal surface (TPMS), namely the Sheet-Diamond topology. First, we employed a series of software including MathMod, Meshmixer, Netfabb and Cura to design the model. Then, we utilized additive manufacturing technology to fabricate the cellular structures with designated scale. Finally, we performed compressive testing to deduce the mechanical properties of each cellular structure. Results showed that, in comparison with the high-porosity group, the yield strength of the low-porosity group was 3 times higher, and the modulus was 2.5 times larger. Our experiments revealed a specific relationship between porosity and Young's modulus of PLA-made Sheet-Diamond TPMS structure. Moreover, it was observed that the high- and low-porosity structures failed through distinctive mechanisms, with the former breaking down via buckling and the latter via micro-fracturing.

Keywords Additive manufacturing (AM/3D printing) · Triply periodic minimal surface (TPMS) · Bioscaffolding

Introduction

Musculoskeletal maladies that result in tissue degeneration have risen as the main reason for disability all around the world [1]. For instance, The Institute for Health Metrics and Evaluation (IHME) had claimed that the disability-adjusted life years (DALYs) caused by musculoskeletal maladies increased to the magnitude of 10^8 in 2014 [1]. DALY is a measure of health loss caused by a disease, which is expressed as the number of years lost due to that disease [1]. Generally, small defects in bones can heal through their self-repairing and regeneration mechanism. For large defects especially those above a critical size however, the healing would require external interventions. This is because large defects would get scarred rather than regenerated, leading to a nonunion growth [2]. Reparation of a massive bone defect obligates bioscaffolds [2].

A bioscaffold is an artificial structure implanted into the human body in order to promote tissue regeneration and injury recovery [3]. Made of biocompatible and/or bioresorbable materials, two kinds of bioscaffolds are commercially available to date. One is derived from human or animal tissues (Fig. 1), and the other is synthesized bioscaffolds (Fig. 2). The former has proven to be expensive, painful, scarring and constrained by anatomical limitations [4]. Besides, this kind of bioscaffolds still has the risk of eliciting an immune response in recipients and/or introducing infection or disease from the donor [4]. On the other hand, synthetic bioscaffolds, for example, truss structures, suffer from unreliable biological fixation due to the surface characteristics of the implant. Synthetic bioscaffolds often have sharp angels that would not only cause poor adhesion onto tissues [5] but also the accumulation of mechanical strain. Excessive mechanical strain can bring about propagating cracks hence the failure of the bioscaffolds.

✉ Zizhen Cai
zizhenc0901@gmail.com

[1] Department of Materials Engineering, Faculty of Applied Science, University of British Columbia, 2329 West Mall, Vancouver, BC V6T 1Z4, Canada

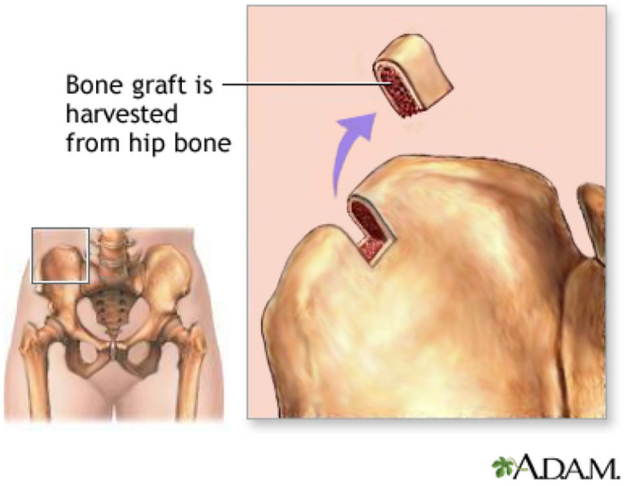

Fig. 1 Illustration of bioscaffolds derived from human hip bone [6]

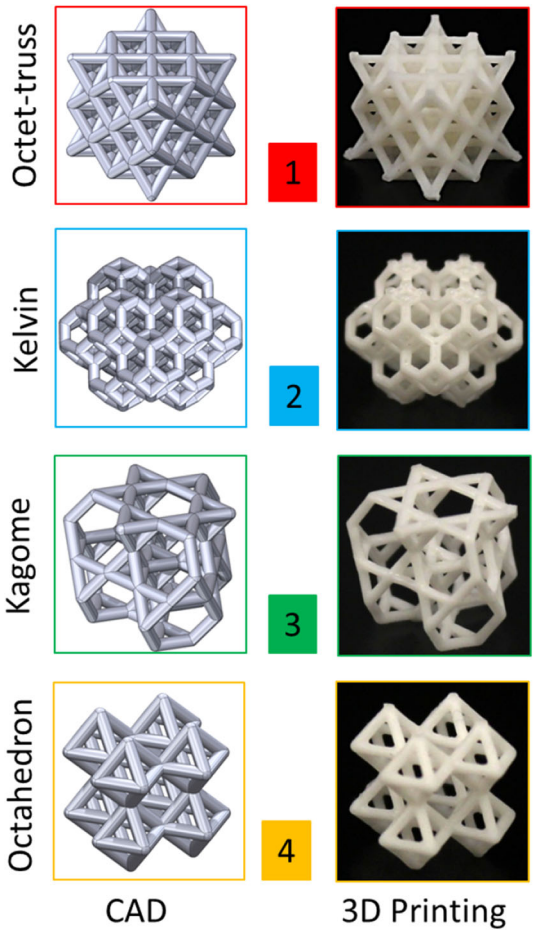

Fig. 2 Truss structure, a type of currently synthesized bioscaffolds [7]

In order to improve the bioscaffolds that are highly desirable in orthopedic operations, especially for patients with bone trauma, cancer, defects or missing bones [8], the following requirements must be fulfilled.

First and foremost, any bioscaffold has to be biocompatible. It must be capable of letting cells migrate and attach to the surface [4]. This lowers the risk of the immune response, avoiding the occurrence of severe inflammation or infection, which would otherwise lead to rejection [4].

Second, bioscaffolds must process the same mechanical properties as the tissue it is implanted into. They have to be strong enough to support the human body post implantation [5], at the same time avoiding stress shielding. Stress shielding refers to the reduction in bone density (osteopenia) as a result of the removal of typical stress from the bone by an implant [8]. According to Wolff's law, a normal bone will remodel itself adjusting to its load [8]. Therefore, a reduction in load will result in the bones becoming thinner and weaker as there is no stimulus for continued remodelling.

Last but not the least, the porosity of bioscaffolds should be close to trabecular bones (ranging from 55 to 90%). High porosity with interconnected pore structure would allow adequate diffusion of nutrients to cells and the growth of tissue and blood vessels.

To meet the above requirements, we set out to search for a bioscaffold structure that best mimics the trabecular bone structure. Comparison of the bone structure and current bioscaffolds, e.g., truss structure, reveals that the real bone structure has an almost continuous surface, while the truss structure does not. We thus focused on the triply periodic minimal surface (TPMS) structure. TPMS, or triply periodic minimal surface, is the repeat one minimal surface [9] that has a crystalline structure, in the sense of three-dimensional periodicity [10]. In our opinion, TPMS's excellent suitability as bioscaffolds lies in its high similarity to human trabecular bone structures, with connected pores to allow tissue growth and smooth joints to alleviate stress [11]. TPMS has the added benefits in terms of its light weightiness and superior energy absorptivity [11]. With a 5 math-based structure, TPMS is also easy to modify. Only a few parameters need to be changed for its structural modification.

The complex cell geometries full of regulated cavities of TPMS present a great challenge for its fabrication especially when the desired size scale gets smaller. Recent advances in additive manufacturing (AM) helped to mitigating these challenges. Additive manufacturing, also known as 3D printing or rapid stereotyping, refers to the process where three-dimensional objects are made directly from digitallmodels (e.g., CAD files) [12]. 3D printing is now widely used in many fields, including engineering designs and manufacturing, architectural designs and biomedical engineering. In biomedical engineering, 3D printing has been used to produce customized artificial tissues such as skull bones and hip implants [13]. One of the commonly used methods is extrusion-based 3D printing, where thermoplastic polymers are heated above the glass transition temperature and extruded to form objects layer by layer. Some of

the commonly used thermoplastics are polycarbonates (PC), polylactic acid (PLA), acrylonitrile butadiene styrene (ABS), with polyethylene oxide terephthalate (PEOT) and polybutylene terephthalate (PBT) being used as biomaterials with special needs [14].

The combination of TPMS and 3D printing presents us with an enticing prospectus that personalized bioscaffolds can be produced based on specific defect sizes and shapes of each patient. In such cases, doctors simply need to accomplish their design by drawing in a computer and exporting it to a 3D printer.

Experimental methods

Parameter determining

Pore size

Our initial study showed that the minimum pore size was around 100 microns taking into consideration the size of the cells and their migration requirement. Subsequent studies, however, showed a larger pore size could enhance bone formation. It was observed that a pore size of around 300–400 microns could have a higher alkaline phosphatase activity and osteocalcin content, as well as better new bone formation. The 300 micron was also the critical size for capillaries formation [15]. Besides, larger-diameter pores favor direct osteogenesis by having better vascularization to enhance oxygen tension and supply of nutrients. Furthermore, when researchers implanted poly (propylene fumarate) scaffolds with two different pore sizes, i.e., 300–500 and 600–800 microns, in rabbits with cranial or subcutaneous defects, no difference was observed in bone formation. Instead, more fibrosis formed with implants of smaller pore sizes, i.e., 300–500 microns. Therefore, pore sizes larger than 500 microns were recommended. In our case, the pore size in the TPMS structures was 8 mm, which was much larger than 500 microns, hence the pore size did not pose a constraint on our design [16].

Porosity

The TPMS structure should have a high porosity to support cell growth, nutrient transport, metabolite discharge, etc., at the same time matching tissue stiffness. The trabecular architecture of bones has a porosity of 50–95% at the end of long bones [17]. In our design, we chose 55% and 80% porosities as the sample porosity. The former was chosen as it was close to the low end of trabecular bone porosities. In addition, it was likely that the actual printing could give a slightly lower porosity than the set value of 55%, making the resultant sample porosity better matching the lowest trabecular bone porosity. Studies also showed that trabecular bones had an average porosity of 79.3% [18]. We, therefore, chose 80% as the higher porosity of our design as it is close enough to the mean porosity of trabecular bones. As stated above, the chosen porosities were suitable for mimicking the complex trabecular bone structures inside the human body, and the difference between the porosities was large enough to allow us to find out a relationship between compressive strength and porosity of TPMS structures. The relationship between Young's modulus and density is predicted by [16]

$$\frac{E}{E_{\mathrm{s}}} = C\left(\frac{\rho}{\rho_{\mathrm{s}}}\right)^{n}$$

where E is Young's modulus, is the density of the structure, and subscript denotes the property of dense solid.

Topology structure

In Ref. [17], Al-Ketan et al. [19] studied the mechanical properties (i.e., Young's modulus, peak stress, plateau stress and toughness) of different TPMS structures. Samples with different structures were manufactured via 3D printing. Each cubical sample consists of 216 unit cells with 7 mm size and has a total length of 42 mm. The actual relative density was calculated, and all samples showed an increase in the relative density. These samples were tested by applying compression perpendicular to the printing direction, and stress–strain responses were extracted and are presented in Fig. 3. For each cell topology, the stress–strain responses for the different relative densities are presented in the same figure.

The mechanical properties were extracted from the stress–strain responses, plotted against the relative density in log–log scale graphs and fitted with a power law. Figure 4 shows Young's modulus, peak stress, plateau stress and toughness as a function of the relative density for all tested samples. Young's modulus is represented by the slope of the linear curve marking the elastic region. Peak stress is the first pick observed in the stress–strain curve, and plateau stress is obtained as the average stress for the values of strain between 20 and 40%, whereas the toughness is obtained as the area under the stress–strain curve up to a 25% strain. The data point for different cell topologies in Fig. 4 was fitted using a power law in the form of $\emptyset_{\mathrm{cellular}} = C\rho^{n}_{\mathrm{relative}}$, where $\emptyset_{\mathrm{cellular}}$ is the mechanical property of the cellular structure, ρ_{relative} is the relative density, and C and n are fitting constants. The fitted parameters are shown in Table 1.

In general, employing the sheets approach yields values of peak and plateau stress that were 1.3–2 times higher than those achieved using skeletal approach for all TPMS topologies. The Sheet-TPMS based topologies showed higher toughness values as compared to the Skeletal-TPMS, with the

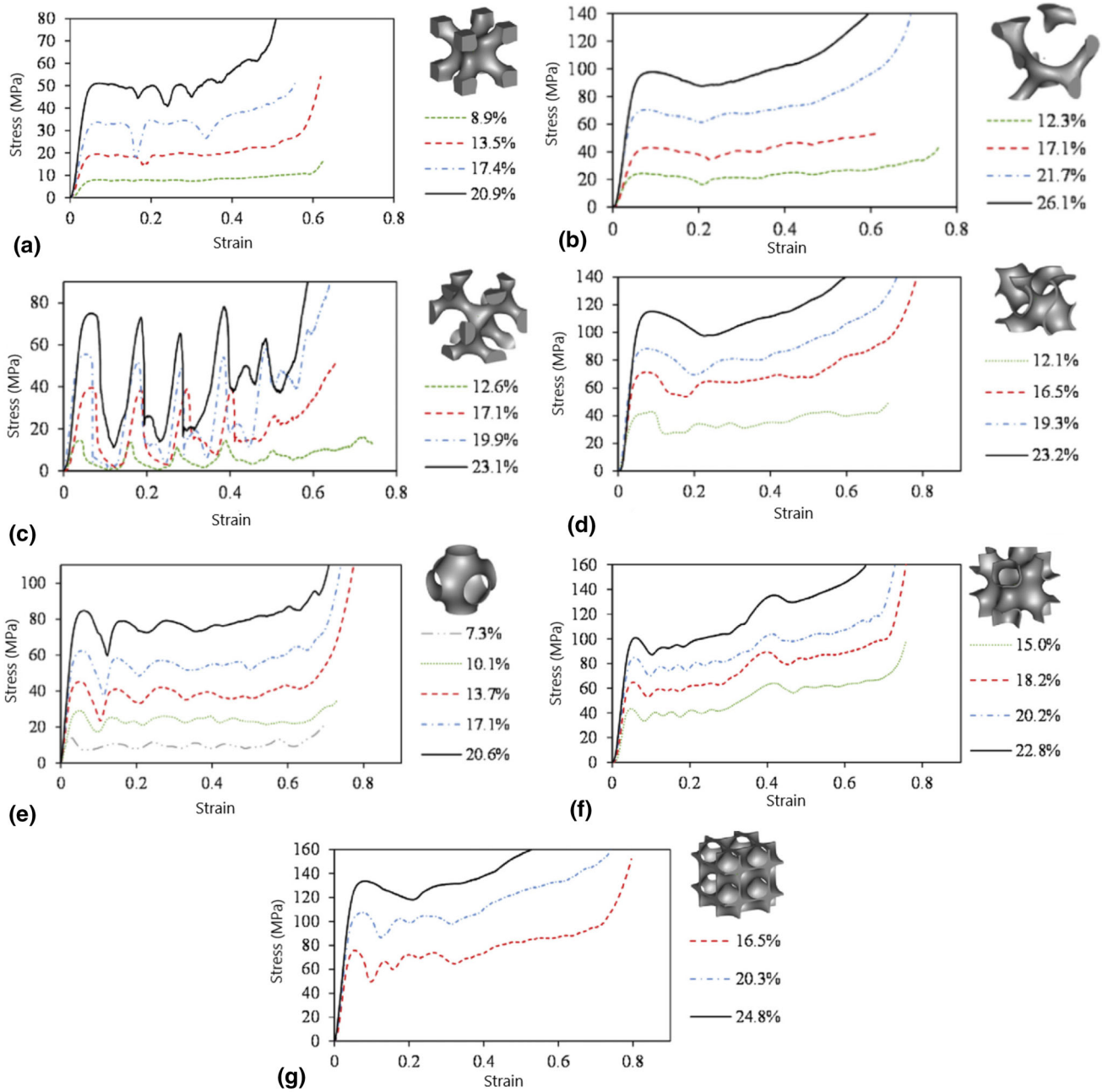

Fig. 3 Stress–strain response of the different cellular structures with different actual printed relative densities. **a** Skeletal-IWP, **b** Skeletal-Diamond, **c** Skeletal-Gyroid, **d** Sheet-Gyroid, **e** Sheet-Primitive, **f** Sheet-IWP, **g** Sheet-Diamond

Sheet-Diamond being the highest. Overall, the Sheet-TPMS based cellular structures showed superior mechanical properties among all the tested structures, and Sheet-Diamond cellular structure performed the best. Therefore, in our design, Sheet-Diamond cellular structure was preferred.

Software designing

In order to design the scaffold made by TPMS, a few designing parameters should be first determined. Since the triply periodic structure is made of a repetition of the unit cells, which are built up with its cell wall and a pore inside it, the size of the pore should be the first designing parameter to be determined, as it potentially affects the biocompatibility of the TPMS-made scaffold. The second designing parameter was the porosity of the whole structure since it can influence both the mechanical and biological properties. The size of the whole structure was relatively arbitrary because it draws from the actual part of the bone for replacement. All other variables were derived from these three parameters. For example, unit

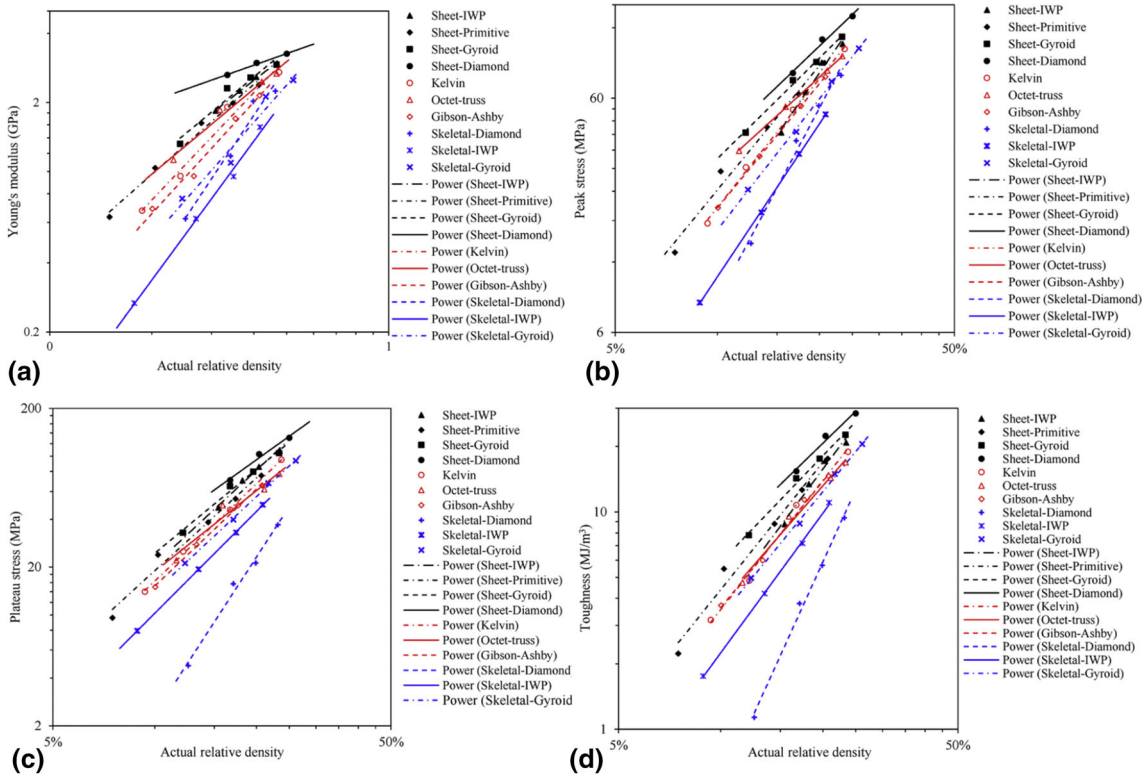

Fig. 4 Deduced mechanical properties of the tested samples. **a** Young's modulus, **b** peak stress, **c** plateau stress and **d** toughness

Table 1 Values of the parameters of the power laws used in fitting the mechanical properties data

	Young's modulus (GPa)		Peak stress (MPa)		Peak stress (MPa)		Toughness (MJ/m^3)	
	C	*n*	*C*	*n*	*C*	*n*	*C*	*n*
Sheet-IWP	15.9	1.15	2354	2.13	1982	1.98	463	2.1
Sheet-Primitive	19.6	1.31	1419	1.77	1667	1.94	391	1.95
Sheet-Gyroid	18.5	1.23	885	1.43	1402	1.76	248	1.62
Sheet-Diamond	6.7	0.522	933	1.39	1112	1.53	237	1.52
Skeletal-Diamond	62.5	2.22	4418	2.73	4566	3.28	1498	3.44
Skeletal-IWP	34.6	2.01	1530	2.17	1389	2.13	305	2.13
Skeletal-Gyroid	24.5	1.68	1189	1.86	1374	1.99	266	1.91

cell size was determined by porosity and pore size, and unit cell number was determined by unit cell size and the size of the structure. However, the designing software was unable to directly adjust the pore size and the porosity. Only the thickness of the cell wall, the size of the structure and the unit cell number were adjustable. Therefore, the desired porosity and pore size were obtained by adjusting unit cell number and cell wall thickness. MathMod is a mathematical modelling software that visualizes and animates implicit and parametric surfaces. The TPMS structure named 'Sheet-Diamond' was visualized by its mathematical equation without a cell wall thickness. By adjusting parameters, there were 5 unit cells on each edge of the cubic structure, and thus, there were in total of 125 unit cells per structure (Fig. 5).

The structure was then exported to Meshmixer. Meshmixer is a 3D designing software which can thicken the surface of a 3D model, thus changing the porosity of the TPMS structure. The thickened TPMS structure was then subsequently exported to another software, Netfabb, to measure its porosity. The unit cell wall thickness continued to be modified until the desired porosity was achieved (Fig. 6).

Finally, the TPMS structure with 125 unit cells and desired porosity were exported to Cura to change the dimensions of the whole structure. One should note that changing the dimensions of the whole structure would also change the

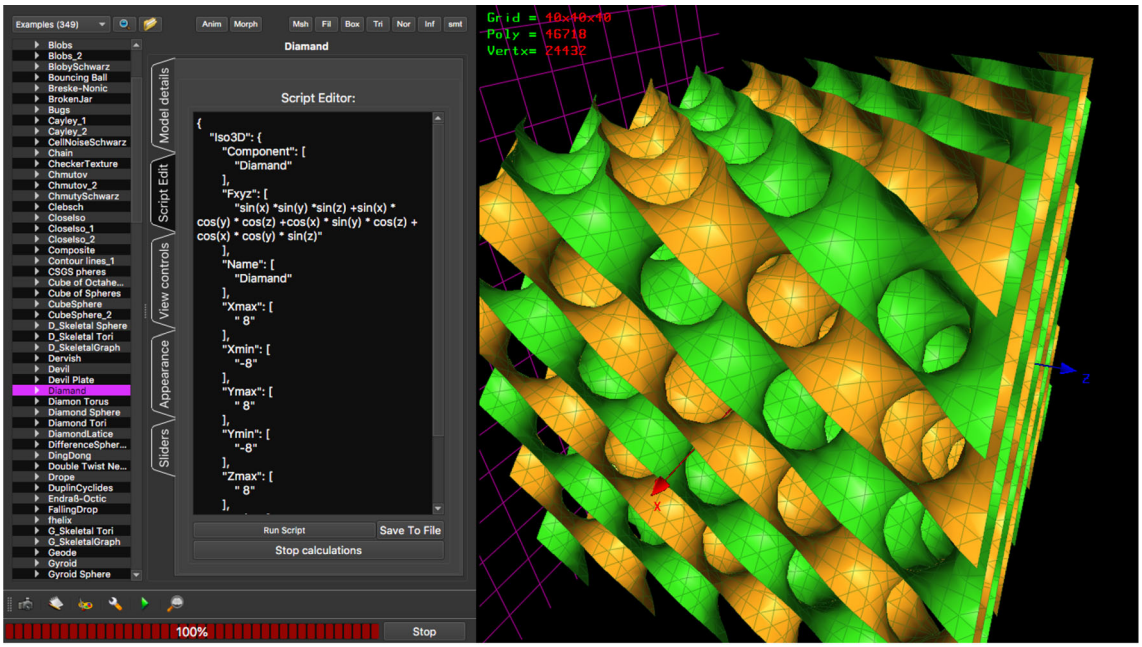

Fig. 5 Model built in MathMod

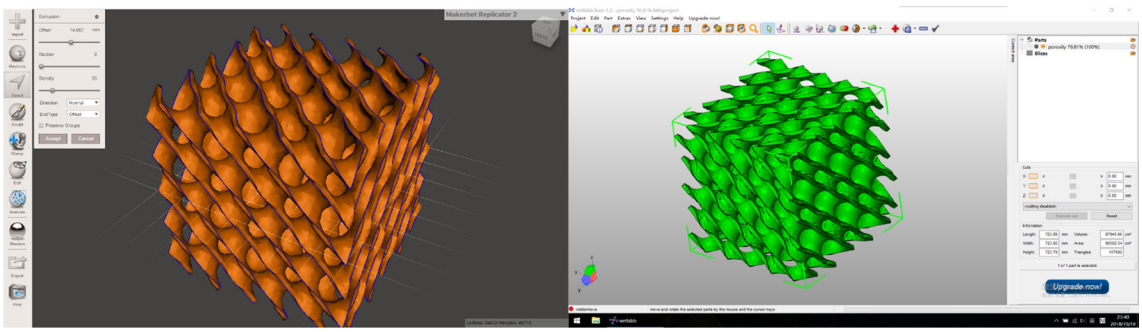

Fig. 6 Model modified in Meshmixer and Netfabb

unit cell size and the pore size because the cell number per edge was fixed (Fig. 7).

Printing

In 3D printing, extrusion temperature has a great effect on the final product. Extrusion temperature refers to the temperature in which filament is extruded by the nozzle of the printer. This temperature affects the flowability of the material and the time needed for the material to cool and settle. For polylactic acid (PLA), which was our printing material, we set the extrusion temperature at 205 °C. This value was obtained through trial and error. Temperature being too low would lead to poor adhesion between the structure and printer plate, which might further result in movements of the structure during printing and separation of layers as shown in Fig. 8. A temperature that was too high would mean PLA could not cool down and harden after being extruded from the printer, and thus some fine PLA filaments could remain in the final structure.

In the printing process, different kinds of printers and printing materials were tried to obtain the best product. At first, the printer Flashforge Creator Pro and fiber-reinforced PLA were used to create the structure, but the product turned out to have a very rough surface possibly due to the carbon fiber particles in the printing material. Next, the printer Monoprice and PLA were chosen. Although a better surface finish was obtained this time, there were some defects at the corner of the structure probably because the stability of the printer was relatively low. In the end, we changed to the printer Ultimaker 2 and still used PLA as the printing material. This combination provided products with smooth surfaces and corners without defects (Fig. 9). Detailed information of polylactic acid (PLA) [20] and technical specifications of Ultimaker 2 [21] can be found in the "Appendix".

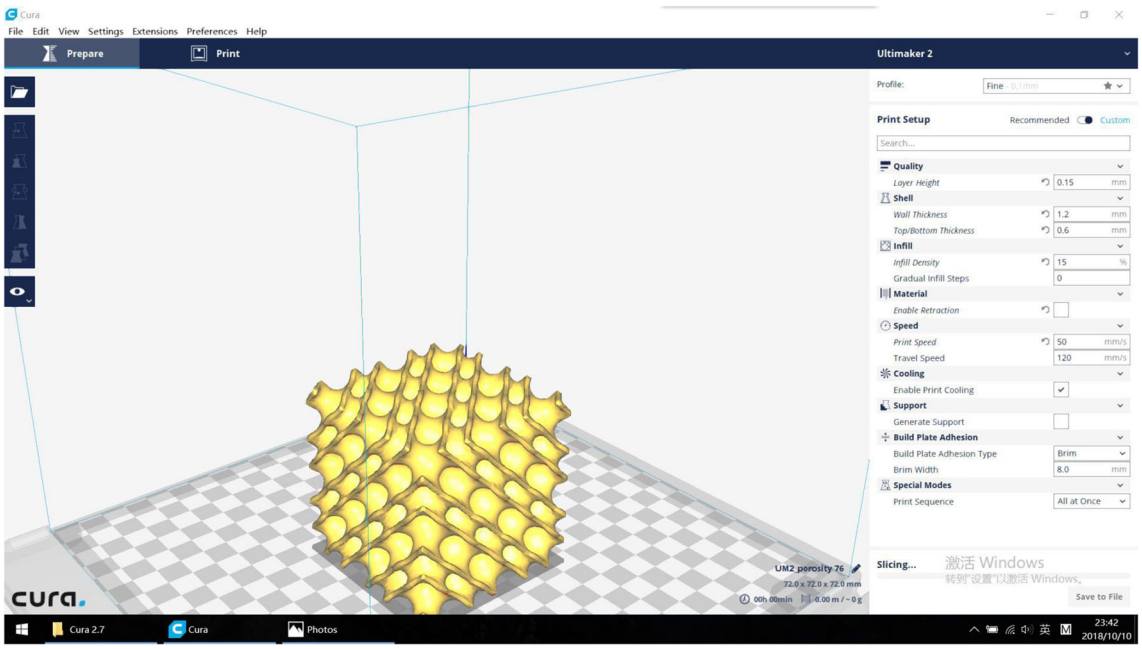

Fig. 7 The dimensions of the whole structure modified in Cura

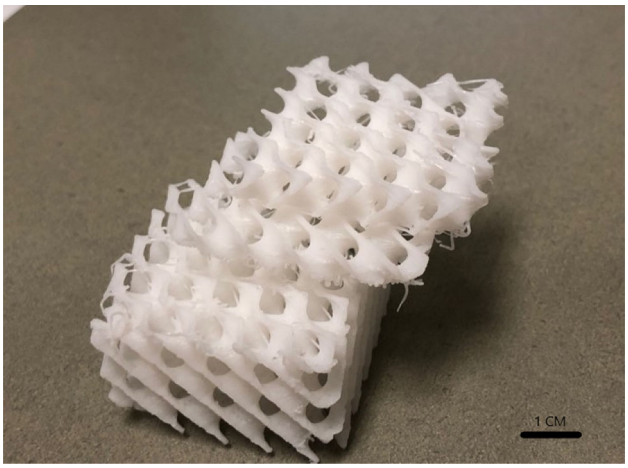

Fig. 8 Separation of layers due to high printing temperature and structure movement during the printing process

Results and analysis

Dimensions measurement

For each sample, the weight and dimensions are measured and listed in Table 2.

Mechanical simulation

Before testing the printed structure, its compressive strength was simulated in Fusion 360. Fusion 360 is a software designed to simulate the mechanical performance of the structure. Since the printed structure does not include flat surfaces at the top and bottom for the force application, two thin plates are placed above and below the structure in the software. The mechanical properties of these two plates were

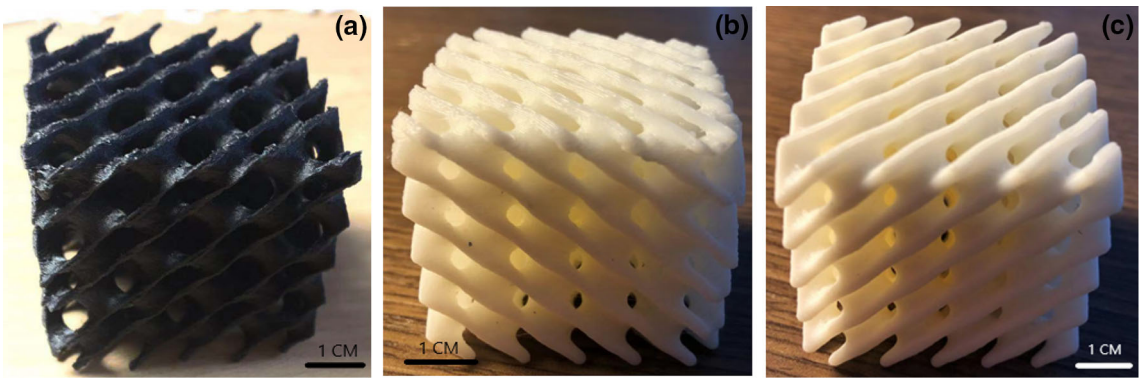

Fig. 9 Structures printed by **a** Flashforge Creator Pro and fiber reinforced PLA, **b** Monoprice and PLA and **c** Ultimaker 2 and PLA

Table 2 Original weight and dimensions measurement

		55% designed porosity Sample 1			55% designed porosity Sample 2			55% designed porosity Sample 3	
Weight (g)		29.41			29.49			29.18	
		29.41			29.49			29.18	
		29.41			29.48			29.18	
Avg weight (g)		29.41			29.4867			29.18	
	Direction 1	Direction 2	Direction 3	Direction 1	Direction 2	Direction 3	Direction 1	Direction 2	Direction 3
Length (mm)	39.61	39.73	39.88	39.64	39.59	39.79	39.61	39.67	39.82
	39.73	39.65	39.90	39.62	39.68	40.00	39.61	39.60	39.88
	39.61	39.70	39.85	39.68	39.63	39.86	39.63	39.60	40.08
Ave length (mm)	39.65	39.69	39.88	39.65	39.63	39.88	39.62	39.62	39.93
Ave length (cm)	3.97	3.97	3.99	3.96	3.96	3.99	3.96	3.96	3.99
		80% designed porosity Sample 1			80% designed porosity Sample 2			80% designed porosity Sample 3	
Weight (g)		12.22			12.12			12.34	
		12.22			12.12			12.34	
		12.23			12.12			12.34	
Avg weight (g)		12.2233			12.12			12.34	
	Direction 1	Direction 2	Direction 3	Direction 1	Direction 2	Direction 3	Direction 1	Direction 2	Direction 3
Length (mm)	39.55	39.54	39.72	39.59	39.64	39.67	39.70	39.52	39.76
	39.60	39.42	39.87	39.60	39.40	39.74	39.54	39.49	39.88
	39.67	39.49	39.90	39.60	39.50	39.71	39.60	39.52	39.72
Ave length (mm)	39.61	39.48	39.83	39.60	39.51	39.71	39.61	39.51	39.79
Ave length (cm)	3.96	3.95	3.98	3.96	3.95	3.97	3.96	3.95	3.98

adjusted to a value much higher than PLA, the material of the TPMS structure to avoid failure due to the plates rather than the simulated structure. However, the yield strength in compressive stress was much lower in simulation than in the compression test. For example, when 1000 N force was applied to the TPMS structure with 55% porosity, the red parts in Fig. 8 indicated the material was yielding. However, the compression test showed that the same sample was able to withstand 15,500 N force before yielding. Also, the simulation showed an asymmetrical failure of the structure, which only yielded on the left side as shown in Fig. 10.

The asymmetrical failure should not occur since the TPMS structure is symmetric. This is confirmed in the compression test in which the structure fails symmetrically. The differences between the simulation and the test result probably arose from the oversimplification of structures in Fusion 360. In designing softwares such as Meshmixer and Cura, the structure is made by over 300,000 surfaces. However, in Fusion 360, the maximum allowed number of surfaces for strength simulation is 10,000. As shown in Fig. 8, many sharp corners and edges appear in the simulated structure, which is not the case in the real printed samples.

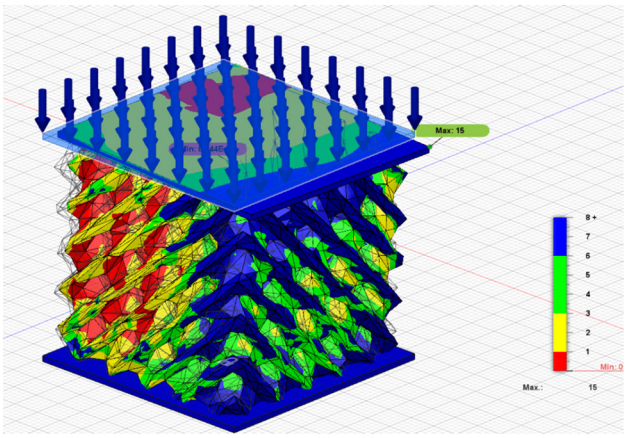

Fig. 10 Simulation result of the TPMS structure with 55% porosity

Compression test

The compression test was done by Instron 3369 Compressive Strength Tester. In the test, the force was applied parallel to the printing direction. The stress–strain curves were drawn automatically by the test system for further analyses.

Table 3 Real porosity of samples with 80% and 55% desired porosity

	80% designed porosity Sample 1	80% designed porosity Sample 2	80% designed porosity Sample 3	80% designed porosity Average
Porosity	0.837815	0.838768	0.836226	$0.838 \pm 1.049 \times 10^{-3}$
	55% designed porosity Sample 1	55% designed porosity Sample 2	55% designed porosity Sample 3	55% designed porosity Average
Porosity	0.612716	0.611151	0.615224	$0.613 \pm 1.678 \times 10^{-3}$

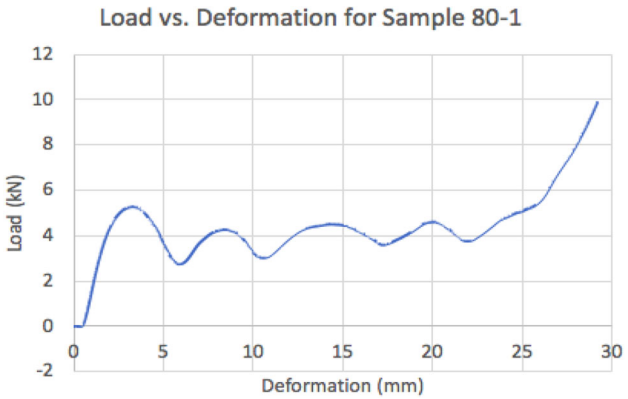

Fig. 11 Load–deformation curve of Sample 1 from 80% porous group

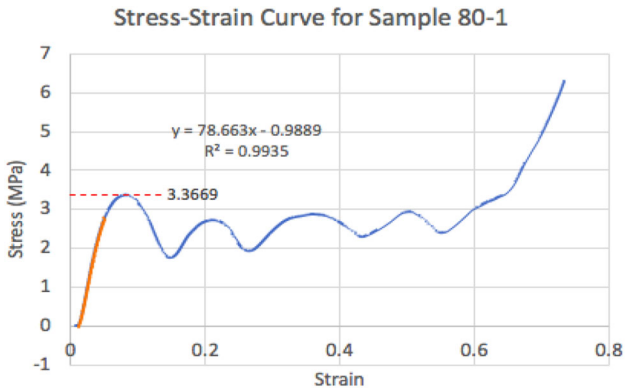

Fig. 12 Stress–strain curve of Sample 1 from 80% porous group

The true porosity is calculated according to the equation

$$\varphi = 1 - \frac{V_{\text{solid}}}{V_{\text{total}}}, \text{ where } V_{\text{solid}} = \frac{\text{Mass}}{\rho_{\text{PLA}}}, \; V_{\text{total}} = L_1 \times L_2 \times L_3.$$

Take $\rho = 1.21$ g/cm^3, the porosities are calculated in Table 3.

The experimentally measured values for the designed group of 80% and 55% porosity are $83.8\% \pm 0.1049\%$ and $61.3\% \pm 0.1678\%$, respectively. Both satisfy the requirements in the range of 50–95% porosity. The compressive test provides a plot of load versus deformation for each sample; Sample 1 from the 80% porous group is taken as an example (Fig. 11).

The stress (MPa) is calculated by

$$\text{Stress (MPa)} = \frac{\text{Load (kN)}}{\text{Area}\left(\text{mm}^2\right)}$$

where the area is the product of the two sides of the surface perpendicular to the printing direction. The strain is calculated by

$$\text{Strain} = \frac{\text{Deformation}}{\text{length of the side along the printing direction}}.$$

From the stress–strain curve, the modulus is calculated as the slope of the straight curve, and the yielding point is labelled as the maximum stress undertaken before plastic deformation, which is 3.3669 MPa for this sample (Fig. 12).

The yield strengths and moduli of the two groups are determined by averaging across each group. As shown in Fig. 13, compared with the 80% porous group, the yield strength of the 55% porous group is approximately 3 times higher, with the modulus being approximately 2.5 times larger.

In addition, the stress–strain curves of the 55% porous and 80% porous groups have different shapes as shown in Fig. 14, indicating their failures dominated by distinctive mechanisms. The structure of relatively low porosity likely failed through micro-fracturing, while that of relatively high porosity presumably failed through buckling [20, 22]. The latter can be attributed to the structural instability, suggestive of a loss of stability as the porosity increases [21, 23]. Therefore, whenever designing a bioscaffold, its porosity should be designated not only similar to that of the damaged tissue but also lower than a certain threshold in order to maintain the stability of the resultant structure. The threshold should be determined case by case through simulation and compressive test, its value depending on the scale, topology and material used (Fig. 14).

The relationship between Young's modulus and density can be described by equation

$$\frac{E}{E_{\text{s}}} = C\left(\frac{\rho}{\rho_{\text{s}}}\right)^n$$

where $\frac{\rho}{\rho_{\text{s}}} = 1 - \varphi$ and s refers to solid [22].

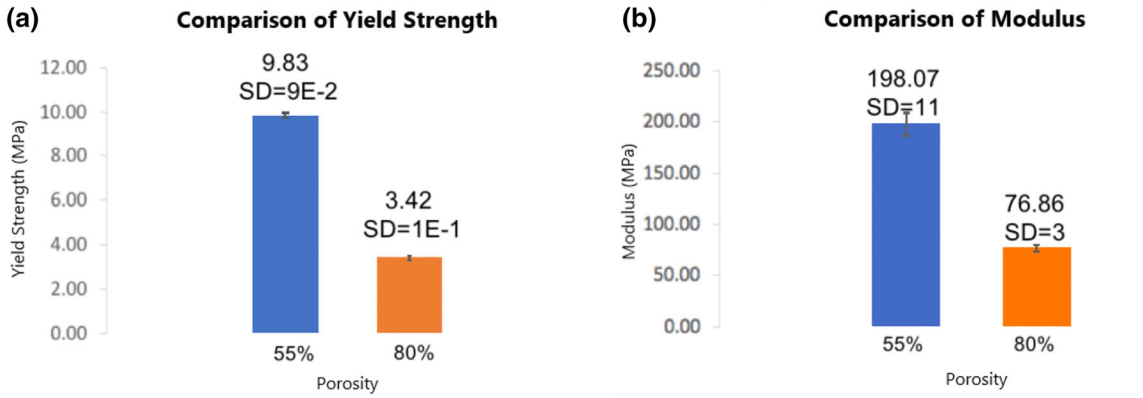

Fig. 13 Comparison of **a** yield strength and **b** modulus between 55% porous group and 80% porous group

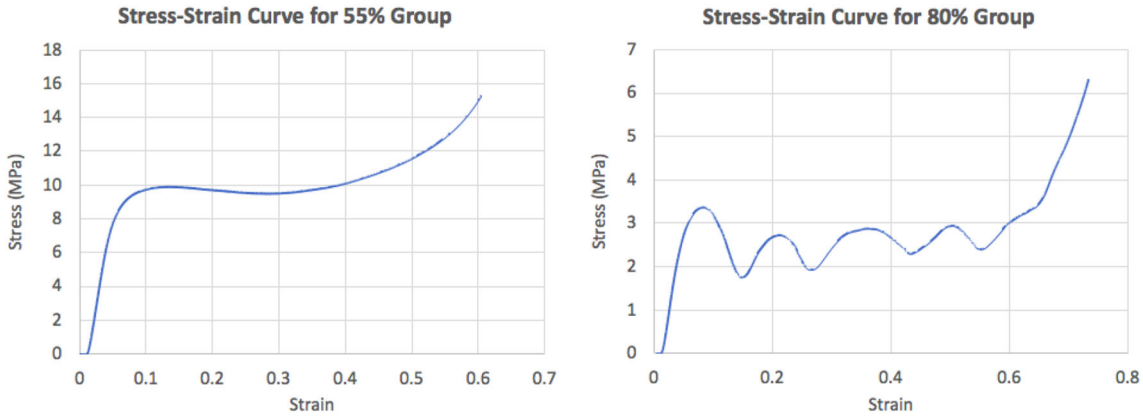

Fig. 14 Comparison of stress–strain curve shape between 55% porous group and 80% porous group

$E_s = 2004.33$ MPa,

Plug in $E = 198.07$ MPa, $\frac{\rho}{\rho_s} = 0.39$ and $E = 76.86$ MPa, $\frac{\rho}{\rho_s} = 0.16$.

Solve for C and n

$C = 0.2687$ and $n = 1.0625$

Therefore, the equation is

$$\frac{E}{E_s} = 0.2687\left(\frac{\rho}{\rho_s}\right)^{1.0625}.$$

This is the relationship between the density and Young's modulus of PLA-made Sheet-Diamond TPMS structure.

Conclusion

In summary, periodic cellular structures with different porosity were designed and fabricated with a selected topology, namely Sheet-Diamond based cellular structures, proving the feasibility of producing the TPMS structure by the 3D printing technique. The fabricated samples were tested by compression and their mechanical properties deduced from the corresponding compressive stress–strain responses. Results showed the yield strength of the low-porosity sample was approximately 3 times higher than that of the high-porosity one, while the modulus of the low-porosity sample was approximately 2.5 times larger than that of the high-porosity one. It was also evident through the stress–strain curves that the low-porosity structures failed through micro-fracturing whereas the high-porosity structures failed through buckling. A mathematical relationship between porosity and Young's modulus of PLA-based Sheet-Diamond TPMS structure was established on the basis of the data obtained, which follows a power law equation.

Limitations

This study covered limited aspects of TPMS structures. In order to get further understandings of TPMS structures in the future, some suggestions are given below:

1. Other types of TPMS structures, like primitive structures, are also worth investigating. Under specific conditions, these structures may give better performances. During the investigation, the researcher should choose several porosities and build different types of TPMS model structures for each porosity. One should also print several samples for compression tests and compare the performances of different types of TPMS structures of different porosities. This way the conditions that other structures perform better than the Sheet-Diamond structure will stand out and the mechanism becomes clear.
2. More data points are needed in order to study the relationship of Young's modulus and porosity of a specific TPMS structure made with that material. Only two porosities are selected in this project, insufficient for interpreting the correlation between Young's modulus and porosity. Selecting more than three porosities for the same TPMS structures to perform a compression test will generate more data points for a more reliable inference on the relationship between Young's modulus and porosity. The more porosities we use, the more accurate that relationship would be.
3. Exploring other materials by performing the same test may help to pinpoint a material that is capable of best mimicking real bone structures. Our current hit, the Sheet-Diamond TPMS structure made by PLA with high porosity, still fails to satisfy the requirements of Young's modulus in a real bone structure at every aspect.
4. Finally, we suggest using a high-speed high-resolution camera for further studies on the failure mechanisms of TPMS structures. Our current recording equipment during the compression tests is a camera from a mobile phone, both the speed and resolution of recording are insufficient for the capture of the detailed process of structural failure. To achieve a thorough understanding of the failure mechanisms of the TPMS structures, we, therefore, propose a dedicated video camera that could help us to rebuild a three-dimensional, time-resolved portrait along the course of structural collapse.

Compliance with ethical standards

Conflict of interest The authors declare that there is no conflict of interest.

Ethical approval This study does not contain any studies with human or animal subjects performed by any of the authors.

Appendix

Detailed information about PLA used during the printing process is presented below:

	Polylactic acid (PLA)
Density	1.00–2.47 g/cc
Additive loading	10.0–40.0%
Tensile strength, ultimate	14.0–114 MPa
Tensile strength, yield	2.00–103 MPa
Modulus of elasticity	0.0850–13.8 GPa
Melting point	90.0–180 °C
Maximum service temperature, air	60.0–240 °C
Processing temperature	190–220 °C
Nozzle temperature	150–235 °C
	Ultimaker 2
Print technology	Fused filament fabrication (FFF)
Maximum power output	221 W
Layer resolution	0.25 mm nozzle: 150–60 micron
	0.4 mm nozzle: 200–20 micron
	0.6 mm nozzle: 400–20 micron
	0.8 mm nozzle: 600–20 micron
XYZ resolution	12.5, 12.5, 5 micron
Feeder type	Geared feeder
Display	Dot-matrix display with click wheel
Print head	Swappable nozzle
Nozzle diameters	0.25, 0.4, 0.6, 0.8 mm (all included)
Build speed	<24 mm^3/s
Nozzle temperature	180–260 °C
Nozzle heat-up time	<2 min
Build plate leveling	Assisted leveling
Build plate	20–100 °C heated glass build plate
Operating ambient temperature	15–32 °C (59–90 °F)

Original load versus deformation curves and stress–strain curves of all samples are listed below:

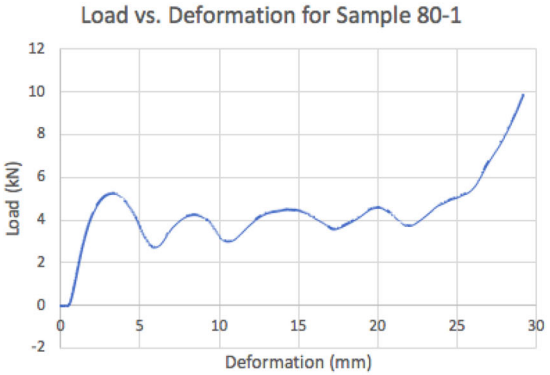

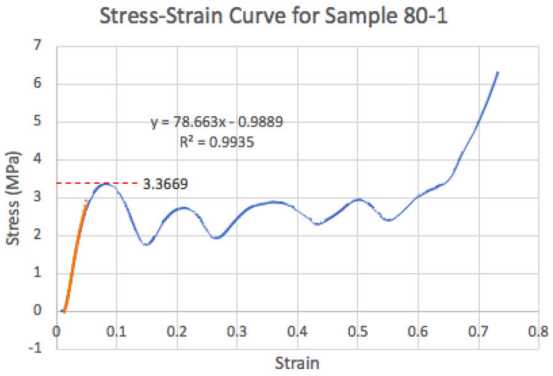

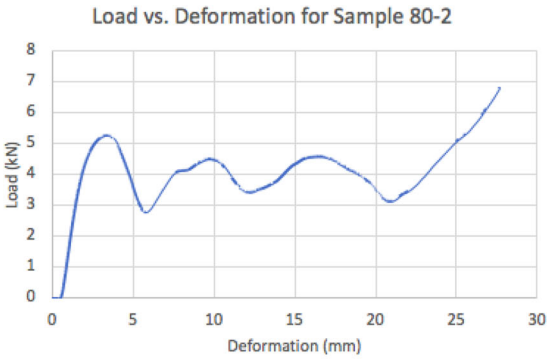

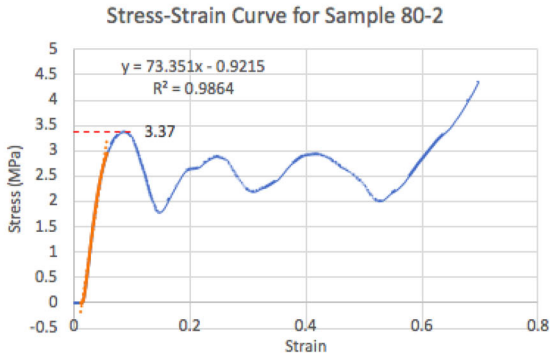

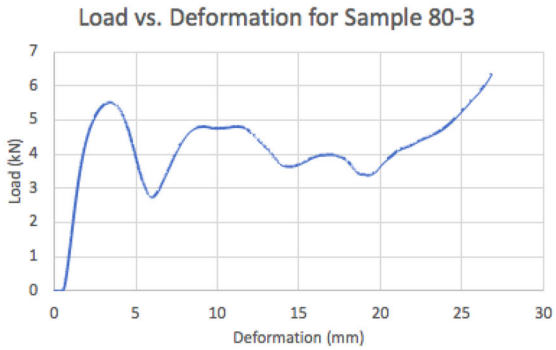

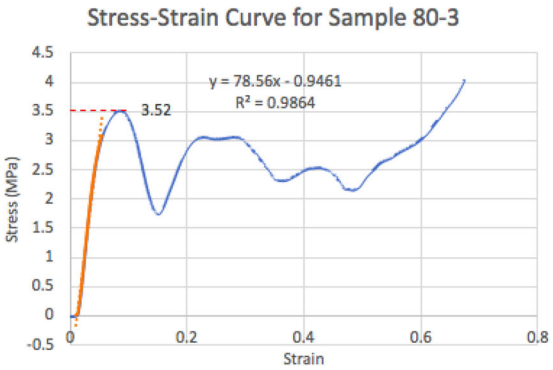

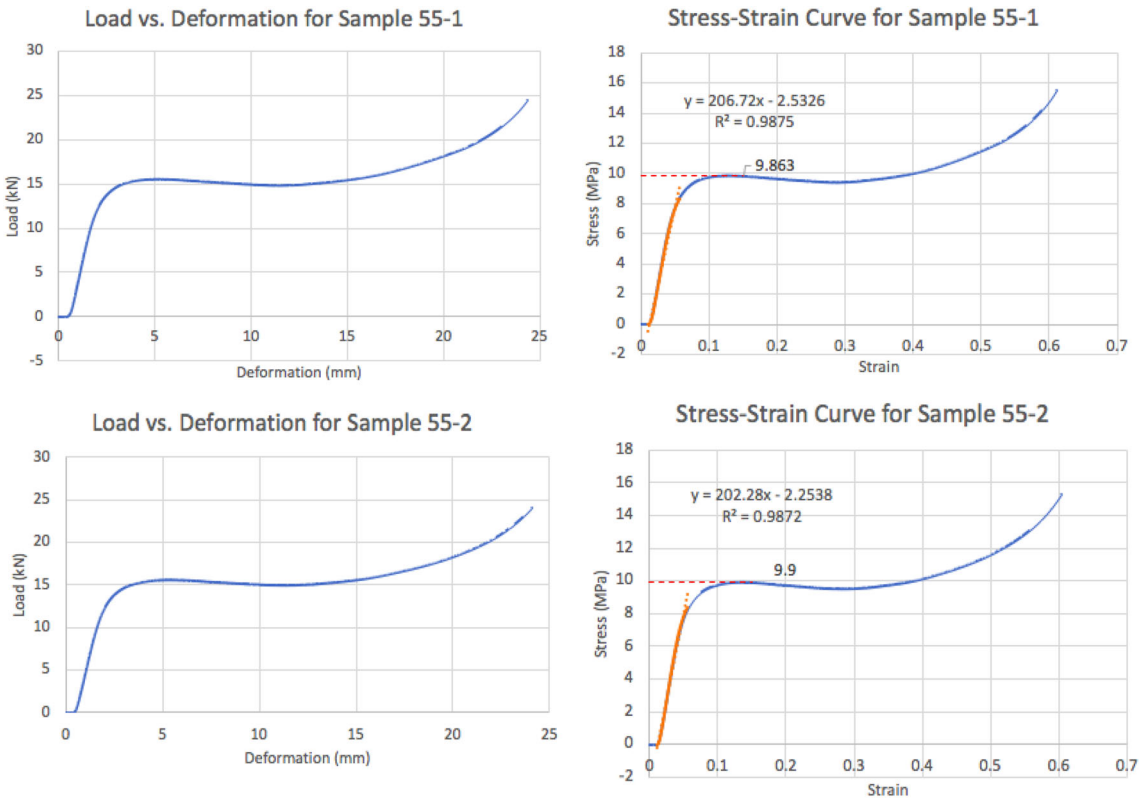

References

1. Yi H, Ur Rehman F, Zhao C, Liu B, He N (2016) Recent advances in nano scaffolds for bone repair. Bone Res 4(1):16050
2. Sandberg O, Aspenberg P (2016) Inter-trabecular bone formation: a specific mechanism for healing of cancellous bone. Acta Orthop 87(5):459–465
3. BioScaffold-Engineered Scaffold for Tissue Engineering—Home (n.d) [EB/OL]. Retrieved from www.bioscaffold.com. Accessed 26 Nov 2018
4. O'Brien FJ (2011) Biomaterials and scaffolds for tissue engineering. Mater Today 14(3):88–95
5. Ataee A, Li Y, Fraser D, Song G, Wen C (2018) Anisotropic Ti–6Al–4V gyroid scaffolds manufactured by electron beam melting (EBM) for bone implant applications. Mater Des 137:345–354
6. Bone graft harvest (2018) [EB/OL]. Retrieved from: https://ssl.adam.com/content.aspx?productId=117&pid=2&gid=8745&site=bestdoctors.adam.com&login=BEST4545. Accessed 26 Nov 2018
7. Elastomer lattices (2019) [EB/OL]. Retrieved from: http://yanhui.world/2019/04/10/Elastomer%20lattice/. Accessed 2 May 2019
8. Stress shielding (n.d.) [EB/OL]. Retrieved from: https://en.wikipedia.org/wiki/Stress_shielding. Accessed 26 Nov 2018
9. Zmrzlikar J (2011) [EB/OL]. Minimal surfaces in biological systems
10. Triply periodic minimal surface (n.d.) [EB/OL]. Retrieved from: https://en.wikipedia.org/wiki/Triply_periodic_minimal_surface. Accessed 26 Nov 2018
11. Maskery I, Sturm L, Aremu A, Panesar A, Williams C, Tuck C, Wildman R, Ashcroft I, Hague R (2018) Insights into the mechanical properties of several triply periodic minimal surface lattice structures made by polymer additive manufacturing. Polymer 152:62–71
12. Luo W, Yang X, Ao N (2016) A review of three dimensional printing technologies for biomaterial applications. Mater Rev 30:81–86
13. Bose S, Vahabzadeh S, Bandyopadhyay A (2013) Bone tissue engineering using 3D printing. Mater Today 16:496–504
14. Maskery I, Sturm L, Aremu A, Panesar A, Williams C, Tuck C, Wildman R, Ashcroft I, Hague R (2018) Insights into the mechanical properties of several triply periodic minimal surface lattice structures made by polymer additive manufacturing. Polymer 152:62–71
15. Murphy C, O'Brien F (2010) Understanding the effect of mean pore size on cell activity in collagen-glycosaminoglycan scaffolds. Cell Adhesion Migr 4(3):377–381
16. Karageorgiou V, Kaplan D (2005) Porosity of 3D biomaterial scaffolds and osteogenesis. Biomaterials 26(27):5474–5491
17. Tripathi Y, Shukla M (2017) Triply periodic minimal surface based geometry design of bioscaffold. IEEE
18. Khan Y, Laurencin CT (2018) [EB/OL]. Regenerative engineering: advanced materials science principles. Retrieved from: https://www.crcpress.com/RegenerativeEngineering-Advanced-Materials-Science-Principles/Khan-Laurencin/p/book/9781498738248. Accessed 15 Oct 2018

19. Al-Ketan O, Rowshan R, Abu Al-Rub RK (2018) Topology-mechanical property relationship of 3D printed strut, skeletal, and sheet based periodic metallic cellular materials. Addit Manuf 19:167–183
20. Matweb [EB/OL]. Retrieved from: http://www.matweb.com/search/DataSheet.aspx?MatGUID=ab96a4c0655c4018a8785ac4031b9278&ckck=1. Accessed 15 Oct 2018
21. Ultimaker 2+ technical specifications [EB/OL]. Retrieved from: https://ultimaker.com/3d-printers/ultimaker-2-plus. Accessed 17 Jul 2019
22. Gibson L, Ashby M (2000) Cellular solids, structure and properties. Cambridge Univ. Press, Cambridge
23. Akin JE (2010) [EB/OL]. Buckling analysis. Retrieved from: https://www.clear.rice.edu/mech403/HelpFiles/FEA_Buckling_analysis.pdf. Accessed 15 Oct 2018